Measuring interdependences in dissipative dynamical systems with estimated Fokker-Planck coefficients

Jens Prusseit[1,2,*] and Klaus Lehnertz[1,2,3,†]

[1]*Department of Epileptology, Neurophysics Group, University of Bonn, Sigmund-Freud-Strasse 25, 53105 Bonn, Germany*

[2]*Helmholtz-Institute for Radiation and Nuclear Physics, University of Bonn, Nussallee 14-16, 53115 Bonn, Germany*

[3]*Interdisciplinary Center for Complex Systems, University of Bonn, Römerstrasse 164, 53117 Bonn, Germany*

(Received 23 November 2007; revised manuscript received 11 February 2008; published 18 April 2008)

We propose a data-driven approach to measure interdependences between dissipative dynamical systems under the influence of noise. We estimate drift and diffusion coefficients of a Fokker-Planck equation and derive measures that allow one to quantify the asymmetry in coupling in a fully automated and computationally inexpensive and simple way. Our approach makes it possible to discriminate between interdependences in the deterministic and stochastic parts of the dynamics. We report results of numerical studies of exemplary time series from coupled stochastic and deterministic model systems and of an application to electroencephalographic recordings from epilepsy patients.

DOI: 10.1103/PhysRevE.77.041914 PACS number(s): 87.19.L−, 05.10.Gg, 05.45.Tp

I. INTRODUCTION

Understanding interdependences between complex dynamical systems is of great importance in nearly all sciences, including physics, chemistry, biology, neurosciences, economy, and even sociology. In many situations the underlying equations of motion are not known, but a detailed quantitative description of interdependences can nevertheless be achieved by applying time-series analysis techniques to experimentally acquired observables. Over the last decades a number of methods have been developed that allow one to detect and to quantify the strength of possible interactions (see [1–4] for an overview). More recently, asymmetric approaches have facilitated the detection of directional coupling from time series. These approaches can be divided into three major groups (for an overview see [5,6]): techniques based on interrelations of the phases of the time series [7–15], state-space-based methods [16–19], and information-theoretic approaches [20–22]. Some of these methods make rather strict assumptions about the dynamics of the systems generating the time series (e.g., linear systems or weakly coupled self sustained oscillators), and many approaches preferentially focus on the low-dimensional deterministic part of the dynamics. The dynamics of many complex systems, however, exhibits deterministic and stochastic features, and nontrivial effects of noise—particularly in nonlinear dynamical systems—are a subject of great interest and importance [23–25].

We here introduce an alternative approach to measure interdependences in dissipative dynamical systems under the influence of dynamical noise. These systems can often be successfully modeled by a Fokker-Planck equation, which reads [26–28]

$$\frac{\partial}{\partial t}p(\mathbf{x},t|\mathbf{x}',t') = \left(-\sum_i \frac{\partial}{\partial x} D_i^{(1)}(\mathbf{x},t) + \sum_{ij} \frac{\partial^2}{\partial x_i \partial x_j} D_{ij}^{(2)}(\mathbf{x},t)\right) p(\mathbf{x},t|\mathbf{x}',t'), \quad (1)$$

where the state of the d-dimensional system is denoted by $\mathbf{x}=(x_1,\ldots,x_d)$ and $p(\mathbf{x},t|\mathbf{x}',t')$ is the conditional probability density to find the system in state $\mathbf{x}$ at time t if it was in state $\mathbf{x}'$ at time t'. An equivalent description of the level of realizations of the process is given by the associated Langevin equation

$$\dot{x}_i = h_i(\mathbf{x},t) + \sum_j g_{ij}(\mathbf{x},t)\Gamma_j(t), \quad (2)$$

where $\Gamma_j(t)$ are uncorrelated Gaussian white noise processes—i.e., $\langle \Gamma_i(t)\Gamma_j(t')\rangle = \delta_{ij}\delta(t-t')$, which have vanishing mean $\langle \Gamma_j(t)\rangle = 0$. The functions h_i describe the deterministic part of the dynamics, and $\mathbf{g}=\{g_{ij}\}$ is a symmetric matrix specifying the strength of the noise. If the entries g_{ij} depend on the state $\mathbf{x}$, the stochastic part is referred to as multiplicative dynamical noise, otherwise as additive dynamical noise. The functions h_i and g_{ij} are related to the drift ($D_i^{(1)}$) and diffusion ($D_{ij}^{(2)}$) coefficients of the associated Fokker-Planck equation via

$$D_i^{(1)}(\mathbf{x},t) = h_i(\mathbf{x},t), \quad (3)$$

$$D_{ij}^{(2)}(\mathbf{x},t) = \sum_k g_{ik}(\mathbf{x},t)g_{kj}(\mathbf{x},t), \quad (4)$$

using Itô's interpretation of stochastic integrals [26].

In Refs. [29–31] an analysis technique has been introduced that allows—for stationary (and ergodic) processes—the estimation of the coefficients $\mathbf{D}^{(n)}$ from time-series data using their statistical definition in terms of the conditional moments $\mathbf{m}^{(n)}$ of the process

$$\mathbf{D}^{(n)}(\mathbf{x}) = \frac{1}{n!}\lim_{\tau\to 0}\frac{1}{\tau}\mathbf{m}^{(n)}(\mathbf{x},\tau), \quad (5)$$

*jprusseit@gmx.de

†klaus.lehnertz@ukb.uni-bonn.de

$$\mathbf{m}^{(n)}(\mathbf{x},\tau) = \langle [\mathbf{X}(t+\tau) - \mathbf{X}(t)]^n \rangle|_{\mathbf{X}(t)=\mathbf{x}}. \quad (6)$$

In the case of the diffusion coefficient ($n=2$) the square has to be evaluated as a dyadic product, and the conditional moments in Eq. (6) are calculated for finite time steps τ and then extrapolated to $\tau=0$. This technique has been successfully applied in a variety of disciplines ranging from physics [32–38] to the biomedical domain [39–41] and, more recently, has been shown to provide valuable information for the diagnosis of epileptic brain dynamics [42]. Moreover, in Refs. [43,44] the proposed time-series analysis technique was extended further to handle both dynamical and measurement noise. We here use this approach to derive measures for interdependences between stochastic processes by investigating the functional dependence of the estimated Fokker-Planck coefficients on the different components of a multidimensional time series.

This paper is organized as follows. In Sec. II we define our measures for interdependences between stochastic processes using the time-series analysis approach introduced in Refs. [29–31]. We show results of numerical studies of exemplary time series from coupled stochastic and deterministic model systems in Sec. III, and in Sec. IV we report on an application of our approach to measure interdependences in electroencephalographic recordings from epilepsy patients and discuss the potential diagnostic relevance of our approach. Finally, concluding remarks are given in Sec. V.

II. DEFINITION OF INTERDEPENDENCE MEASURES

To characterize interactions between stochastic processes we estimate the drift and diffusion coefficients of the corresponding Fokker-Planck equation of the process from empirical data [cf. Eqs. (5) and (6)]. We then derive interdependence measures by investigating the functional dependence of the estimated Fokker-Planck coefficients on the different components of a multidimensional time series in a fully automated and computationally inexpensive way. For this purpose we consider two time series x_1 and x_2 as a realization of a two-dimensional (Markovian) stochastic process (generalization to higher dimensions is straightforward) and define measures quantifying the asymmetry in the coupling between the components of this process. Interdependence can result from (a) a coupling in the components of the drift vector describing the deterministic part of the dynamics—i.e., $D_i^{(1)}(x_j) \neq \text{const}$ for a fixed x_i and $i \neq j$, (b) a coupling in the components of the diffusion matrix describing the stochastic part of the dynamics such that the diagonal elements $D_{ii}^{(2)}$ depend on the components x_j $(i \neq j)$, and (c) a coupling in the stochastic part such that $D_{ij}^{(2)} \neq 0$ holds for the off-diagonal elements of the diffusion matrix. When taking into account the relationship between $\mathbf{D}^{(2)}$ and the function $\mathbf{g}$ in the Langevin equation [cf. Eq. (4)]—i.e., $D_{11}^{(2)}=g_{11}^2+g_{12}^2$, $D_{22}^{(2)}=g_{12}^2+g_{22}^2$, and $D_{12}^{(2)}=g_{11}g_{12}+g_{12}g_{22}$—it becomes obvious that for case (b) couplings can be present in both the diagonal and off-diagonal elements of $\mathbf{g}$. Moreover, the requirement of nonvanishing elements $D_{ij}^{(2)}$ in case (c) only holds for $g_{ij} \neq 0$, which leads to a mixture of the two noise processes Γ_1 and Γ_2 in the Langevin equation. In this case, both components of the process are driven by the same noise processes, which could be related to phenomena such as stochastic synchronization [25].

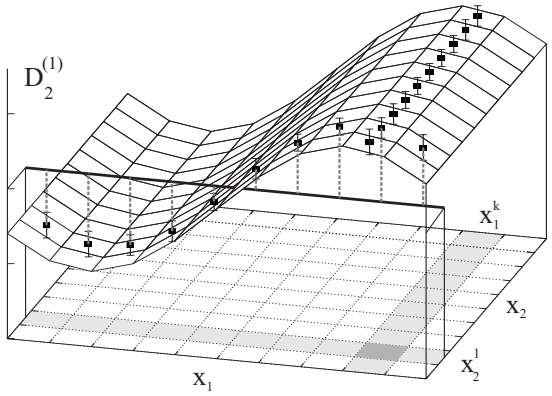

FIG. 1. Schematic of the second component $D_2^{(1)}(x_1,x_2)$ of a hypothetical drift vector. Black squares and error bars indicate estimates for $D_2^{(1)}(x_1^k,x_2^l)$ and their statistical errors for fixed values of x_1^k and x_2^l. The solid horizontal line indicates the error-weighted average μ_l^w of the values of the coefficient over all bins in x_1 direction for a fixed value of x_2^l. The dashed vertical lines are the distances of these values from μ_l^w.

In order to exemplify our approach we show, in Fig. 1, a schematic for the second component $D_2^{(1)}(x_1,x_2)$ of a hypothetical drift vector that varies in the x_1 direction only [see Ref. [45] for an example of coefficients $\mathbf{D}^{(n)}(x_1,x_2)$ derived from empirical data]. For estimating $D_2^{(1)}(x_1,x_2)$ from time-series data [cf. Eq. (5)] we first divide the (x_1,x_2) plane into B^2 bins, and whenever the trajectory of the process hits a certain bin—say, (x_1^k,x_2^l)—we calculate the increment $I_{kl}^{(x_2)} = \frac{1}{\tau}[x_2(t+\tau)-x_2(t)]$ in the direction of x_2. For a fixed time shift τ we then estimate $D_2^{(1)}(x_1^k,x_2^l)$ as the mean value of the distribution of increments in bin (x_1^k,x_2^l) and its statistical error $E[D_2^{(1)}(x_1^k,x_2^l)]$ as the standard error of that mean.

Now, in order to determine the dependence of $D_2^{(1)}(x_1,x_2)$ on x_1—indicating that x_1 couples to the deterministic evolution of x_2—we proceed as follows. For each x_2^l we calculate the weighted average $\mu_l^w[D_2^{(1)}(x_1,x_2)]=\Sigma_k w_k D_2^{(1)}(x_1^k,x_2^l)/\Sigma_k w_k$ over all bins in the x_1 direction where the inverses of the statistical errors are used as weights, i.e., $w_k = 1/E[D_2^{(1)}(x_1^k,x_2^l)]$, and then average over error-weighted distances according to

$$\Delta_l = \frac{1}{n_l}\sum_k \frac{|D_2^{(1)}(x_1^k,x_2^l) - \mu_l^w[D_2^{(1)}(x_1,x_2)]|}{E[D_2^{(1)}(x_1^k,x_2^l)]}, \quad (7)$$

where n_l denotes the number of bins in the x_1 direction for which at least L increments could be calculated. We finally average over all bins in the x_2 direction, and with $F_{2\leftarrow 1}^{(1)} = 1/n\Sigma_l\Delta_l$ (n denotes the number of x_2^l values for which $\Delta_l \neq 0$) we measure the dependence of $D_2^{(1)}$ on x_1. Note that the superscript of $F_{2\leftarrow 1}^{(1)}$ relates to the drift coefficient and with the subscripts we indicate the dependence of the second component of the drift vector on the first component of the process. With the opposite dependence, which is defined in

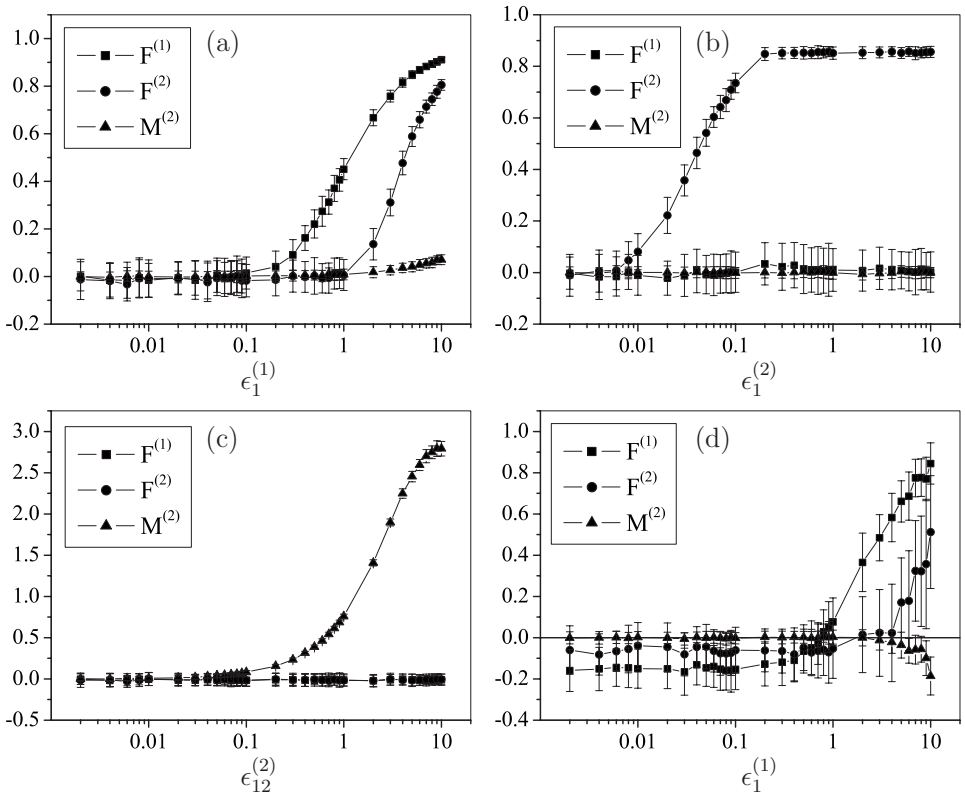

FIG. 2. Dependence of $F^{(1)}$, $F^{(2)}$, and $M^{(2)}$ on the coupling strength. (a) Coupling in the deterministic part, (b) coupling in the stochastic part, (c) mixing of the noise processes, and (d) bidirectional coupling in the deterministic part with fixed $\epsilon_2^{(1)}=0.7$. Symbols and error bars denote means and standard deviations derived from 100 realizations of the respective processes. Time series consisted of $N=50\,000$ data points. Parameters in Eq. (11): $\alpha=\beta=0.1$ for (a)–(c) and $\alpha=3$, $\beta=1$ for (d); $g_{11}=g_{22}=0.1$, $g_{12}=0.01$.

complete analogy, we define a normalized measure for a *coupling in the deterministic part* of the dynamics as

$$F^{(1)} = (F^{(1)}_{1\leftarrow 2} - F^{(1)}_{2\leftarrow 1})/(F^{(1)}_{1\leftarrow 2} + F^{(1)}_{2\leftarrow 1}). \tag{8}$$

$F^{(1)}$ is confined to the interval $[-1;1]$ with positive values indicating a stronger influence of x_2 on x_1 and negative values a stronger influence of x_1 on x_2. A value close to zero can either indicate the absence of interdependences or mutual influences of the two components of the process with comparable strengths. We note that in the latter case an observable of the form $2F^{(1)}_{1\leftarrow 2}/(F^{(1)}_{1\leftarrow 2}+F^{(1)}_{2\leftarrow 1})$ can help to distinguish between these cases. Proceeding in the same way with the diagonal elements of the estimated diffusion coefficient we define—in complete analogy—a normalized measure for a *coupling in the stochastic part* of the dynamics as

$$F^{(2)} = (F^{(2)}_{11\leftarrow 2} - F^{(2)}_{22\leftarrow 1})/(F^{(2)}_{11\leftarrow 2} + F^{(2)}_{22\leftarrow 1}). \tag{9}$$

Finally, by calculating the average value of the off-diagonal element of the estimated diffusion coefficient in units of its statistical error we define a measure that allows one to detect a *mixing of the noise processes* as

$$M^{(2)} = \frac{1}{n_B}\sum_{ij} D^{(2)}_{12}(x_1^i, x_2^j)/E[D^{(2)}_{12}(x_1^i, x_2^j)], \tag{10}$$

where n_B denotes the total number of bins that were hit at least L times by the trajectory of the process.

III. APPLICATION TO MODEL SYSTEMS

A. Two-dimensional diffusion processes

We first present our findings obtained from an analysis of time series that were generated by numerically integrating two-dimensional Langevin equations [46] of the form

$$\dot{x}_1 = f_1(x_1) + \epsilon_1^{(1)}x_2 + (g_{11} + \epsilon_1^{(2)}x_2)\Gamma_1 + \epsilon_{12}^{(2)}g_{12}\Gamma_2,$$

$$\dot{x}_2 = f_2(x_2) + \epsilon_2^{(1)}x_1 + \epsilon_{12}^{(2)}g_{12}\Gamma_1 + (g_{22} + \epsilon_2^{(2)}x_1)\Gamma_2, \tag{11}$$

where $f_1(x_1)=-\alpha x_1$, $f_2(x_2)=x_2(\beta-x_2^2)$, and $g_{ij}=$const. Different choices of the coupling strengths ϵ allowed us to simulate the different types of couplings described above, to choose their directions, and to vary their strength. The system was integrated using a stochastic Euler scheme with an internal time step of 0.001. For the analyses the time series were down-sampled by a factor of 10 and normalized to zero mean and unit variance. We note that our measures do not depend on the chosen normalization, since the estimated coefficients enter Eqs. (7)–(10) in units of their statistical errors only. Time series consisted of $N=50\,000$ data points. We partitioned the state space using $B=10$ bins per dimension and required a minimum number of entries per bin of $L=100$ [47]. For each value of the coupling strength we generated 100 independent realizations of the respective processes and used a fixed time shift of $\tau=1$ sampling interval for the estimation of the coefficients to allow a fully automatized analysis.

In Fig. 2(a) we present results obtained for a unidirectional coupling of x_2 into the deterministic part of the equation of motion of x_1 (i.e., all coupling strengths were zero except $\epsilon_1^{(1)}$). $F^{(1)}$ correctly detected the direction of the cou-

pling (positive values) and allowed us to quantify its strength for a large range of coupling strengths (about two orders of magnitude before it saturates to a value close to 1). $F^{(2)}$ and $M^{(2)}$ only detected a coupling at larger values of $\epsilon_1^{(1)}$), which can be explained by the finite time step used for estimating the coefficients [48–50]. This leads to $O(\tau^2)$ contributions in the second moment $\mathbf{m}^{(2)} = \langle [\mathbf{X}(t+\tau) - \mathbf{X}(t)]^2 \rangle|_{\mathbf{X}(t)=\mathbf{x}}$ that are functions of $\mathbf{D}^{(1)}$ and thus contain the coupling (see the Appendix). Nevertheless, for a relatively wide range of $\epsilon_1^{(1)}$ values ($0.1 \leq \epsilon_1^{(1)} \leq 1.0$) an identification of the coupling in the deterministic part was possible. For a unidirectional coupling of x_2 into the first diagonal element of the stochastic part of the equation of motion of x_1 (i.e., all coupling strengths were zero except $\epsilon_1^{(2)}$) we obtained qualitatively similar results [cf. Fig. 2(b)]. $F^{(2)}$ turned out to be sensitive to weaker couplings, and the range of the coupling strength that could be resolved before the measure saturated to a value close to 1 was about 1.5 orders of magnitude. Furthermore, for the whole range of $\epsilon_1^{(2)}$ values investigated here a clear identification of the coupling in the diagonal element of the stochastic part of the dynamics was possible since $F^{(1)} \cong 0$ and $M^{(2)} \cong 0$ within the range of errors. In the case of a mixing of the noise processes (i.e., all coupling strengths were zero except $\epsilon_{12}^{(2)}$) our measures were able to clearly identify this type of coupling [Fig. 2(c)]. $F^{(1)}$ and $F^{(2)}$ attained values close to zero (within the range of errors) for the whole range of $\epsilon_{12}^{(2)}$ values, while $M^{(2)}$ allowed us to quantify the coupling for $\epsilon_{12}^{(2)} > 0.1$. For a bidirectional coupling of the two process components in the deterministic part of the dynamics (i.e., all coupling strengths were zero except $\epsilon_1^{(1)}$ and $\epsilon_2^{(1)}$) our findings show that the direction of the dominating coupling can be identified [cf. Fig. 2(d)]. We note that a parameter adjustment [cf. Eq. (11)] was necessary to guarantee stability of the simulated system, particularly for strong couplings. Fixing the coupling strength $\epsilon_2^{(1)} = 0.7$ we observed negative values of $F^{(1)}$ for $\epsilon_1^{(1)} < 0.7$ and positive values for $\epsilon_1^{(1)} > 0.7$. As can be expected from our findings for a unidirectional coupling [cf. Fig. 2(a) and the Appendix], $F^{(2)}$ showed a similar dependence; however, it attained lower values than $F^{(1)}$. $M^{(2)}$ fluctuated around zero within the range of errors.

We next study the influence of the number of data points, N, of the time series on our interdependence measures. As examples, we show in Fig. 3(a) results for $F^{(1)}$ in the case of a coupling of x_2 into the deterministic part of the equation of motion of x_1, in Fig. 3(b) for $F^{(2)}$ in the case of a coupling of x_2 into the first diagonal element of the stochastic part, and in Fig. 3(c) for $M^{(2)}$ in the case of a mixing of the noise processes. As expected, the sensitivity of $F^{(1)}$ and $F^{(2)}$ to weaker couplings decreased with a decreasing number of data points, accompanied by an increase of the statistical spread. Nevertheless, we were able to identify the type of coupling and to quantify its asymmetry from time series consisting of as few as $N = 5000$ data points. For time-series sizes of less than $N = 5000$ data points the direction of coupling can still be detected with $F^{(1)}$ and $F^{(2)}$ for large coupling strength, but the statistical spread of the measure values becomes very large (results not shown here). In the case of a mixing of the noise processes the sensitivity of $M^{(2)}$ did not seem to depend on the number of data points N [cf. Fig. 3(c)]. Only the statistical spread of $M^{(2)}$ increased with decreasing N, and we were able to resolve a range of coupling strengths of about two orders of magnitude even with as few as $N = 1000$ data points.

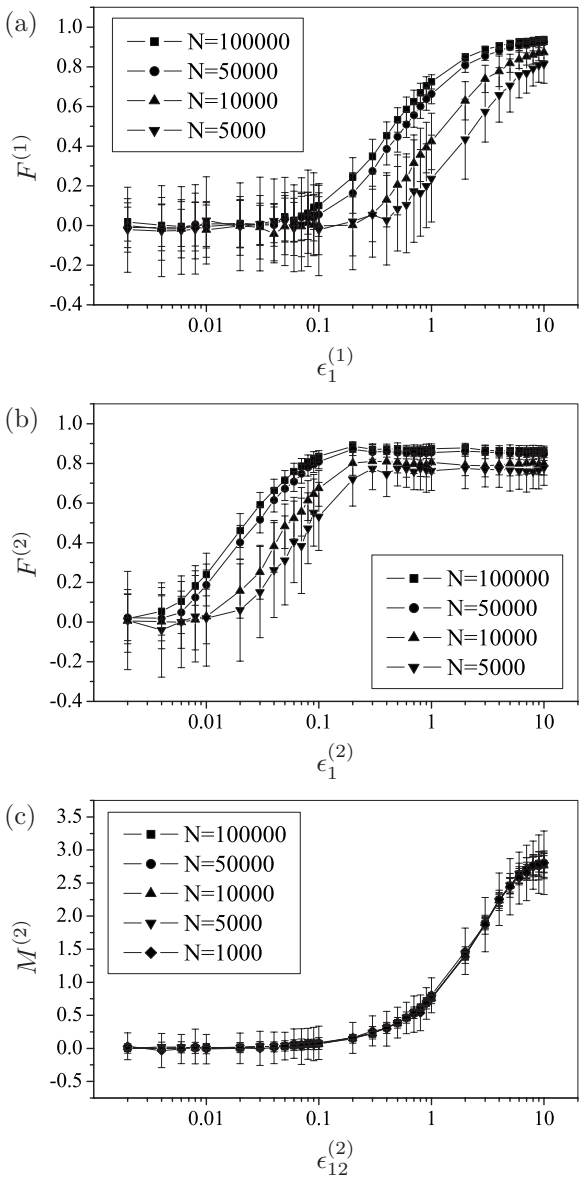

FIG. 3. Dependence on the coupling strength of $F^{(1)}$ in the case of a unidirectional coupling in the deterministic part (a), of $F^{(2)}$ in the case of a unidirectional coupling in the diagonal element of the stochastic part (b), and of $M^{(2)}$ in the case of a mixing of the noise processes (c) for different sizes N of the analyzed time series. Symbols and error bars denote means and standard deviations derived from 100 realizations of the respective processes. $B = 10$, $L = 100$, and parameters in Eq. (11): $\alpha = \beta = 0.1$, $g_{11} = g_{22} = 0.1$, and $g_{12} = 0.01$.

B. Higher-dimensional deterministic model system

We next consider the case of higher-dimensional deterministic systems that do not meet the prerequisites needed for an analysis in terms of a two-dimensional Fokker-Planck equation. As an example for such systems, we here consider coupled Rössler dynamics (cf. [51–53])

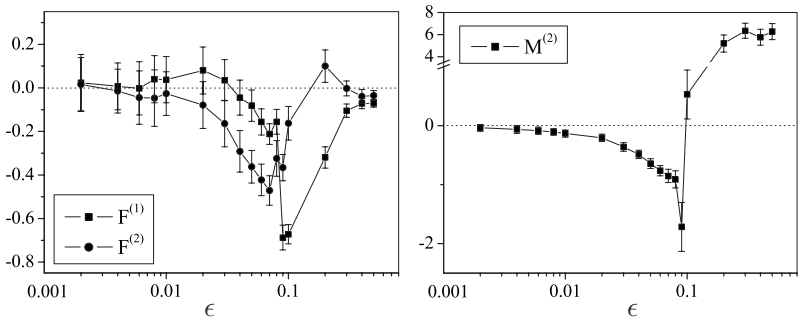

FIG. 4. Dependence of $F^{(1)}$ and $F^{(2)}$ (left) and $M^{(2)}$ (right) on the coupling strength ϵ for two coupled Rössler dynamics. Symbols and error bars denote means and standard deviations derived from 100 realizations of the respective processes [cf. Eq. (12)]. Time series consisted of $N=10\,000$ data points. Note the break in the ordinate in the plot of $M^{(2)}$.

$$\dot{x}_1 = -\omega_x x_2 - x_3,$$

$$\dot{x}_2 = \omega_x x_1 + 0.15 x_2,$$

$$\dot{x}_3 = (x_1 - 10)x_3 + 0.2,$$

$$\dot{y}_1 = -\omega_y y_2 - y_3 + \epsilon(x_1 - y_1),$$

$$\dot{y}_2 = \omega_y y_1 + 0.15 y_2,$$

$$\dot{y}_3 = (y_1 - 10)y_3 + 0.2, \tag{12}$$

with $\omega_{x,y}=1\mp\nu$ with $\nu=0.03$. As already shown in Ref. [53] for this value of the frequency mismatch both phase synchronization and generalized synchronization arise at the same magnitude of the coupling strength ϵ. For each value of ϵ we generated 100 realizations by randomizing the initial conditions near the attractor of the systems and discarded the first 10 000 data points to account for possible transients. The systems were integrated using a fourth-order Runge-Kutta scheme with an internal step size of $\Delta t_{int}=0.05$, and the time series were sampled with a sampling interval of $\Delta t=0.3$. For the analysis the components x_1 and y_1 were used as observables and their time series consisted of $N=10\,000$ data points. Again we used $B=10$, $L=100$, and a fixed time shift of $\tau=1$ sampling interval.

As shown in Fig. 4 the asymmetric measures $F^{(1)}$ and $F^{(2)}$ allowed us to detect the correct coupling direction. At a coupling strength of $\epsilon=\epsilon_s\approx 0.1$ the two systems synchronize [53] and $F^{(1)}\to 0$ and $F^{(2)}\to 0$ for stronger couplings. $F^{(2)}$ was more sensitive to the coupling than $F^{(1)}$ and thus allowed us to resolve a larger range of coupling strengths. The symmetric measure $M^{(2)}$ also detected the coupling and attained increasingly negative values with increasing coupling strength. For $\epsilon\geq\epsilon_s$ we observed an abrupt change of the sign and a rapid increase of $M^{(2)}$ toward large positive values. Whether this effect can be used for a characterization of certain synchronization properties needs further investigation.

Summarizing this section, we conclude that our data-driven approach enables a characterization of interactions between stochastic processes and allows one to differentiate between couplings in the deterministic and the stochastic part of the dynamics. Moreover, our findings indicate that even in the case of a violation of the assumption of a two-dimensional diffusion process our approach can still yield valuable information on the presence and the direction of couplings between dynamical systems. The calculation of our measures is computationally very inexpensive. The algorithm is of order $O(N)$, and the calculation of the measures takes about 0.1 s on a desktop computer (clock speed 1.73 GHz) for time series of size $N=50\,000$ data points. Our approach might thus be advantageous for field applications that aim at an investigation of interactions between complex systems with poorly understood dynamics. Such an investigation will be presented in the next section.

IV. APPLICATION TO EEG DATA

Surgical treatment of focal epilepsies requires exact localization of the seizure generating area of the brain (epileptic focus) and its delineation from eloquent cortex, which is indispensable for defined cortical functions [54]. Although the concept of an epileptic focus has been successful in epilepsy surgery, there is now evidence for this concept to be replaced by a more complex model, which takes into account potential interactions within the neural networks involved in seizure generation [55–58]. In this context, gaining deeper insights into the directionality of possible interactions between different brain regions—even during seizure-free periods—may help to improve understanding of the basic mechanism that lead to the generation of epileptic seizures. Since the 1970s linear interdependences among EEG signals have been analyzed by cross correlation in time domain [59,60] and by cross spectrum or coherence in frequency domain [61,62]. More recently, approaches based on asymmetries of nonlinear interdependence measures [17,57,63–66], of phase relationships [13,14,67], or of entropy-based estimators of information flow [21] have been proposed, and exemplary investigations indicate that directional interdependences in the epileptic brain can be assessed. As already mentioned in the Introduction, however, most of these methods make rather strict assumptions about the dynamics of the underlying systems and many approaches preferentially focus on the low-dimensional deterministic part of the dynamics. In contrast, in a previous study [42] we showed that valuable information for diagnostic purposes can be obtained particularly when considering stochastic and high-dimensional influences on brain dynamics.

We here retrospectively studied multichannel, multiday electroencephalographic (EEG) recordings from eight patients suffering from pharmacoresistant focal epilepsies of temporal lobe origin. These data were already investigated in Ref. [42] using qualifiers that were based on estimated

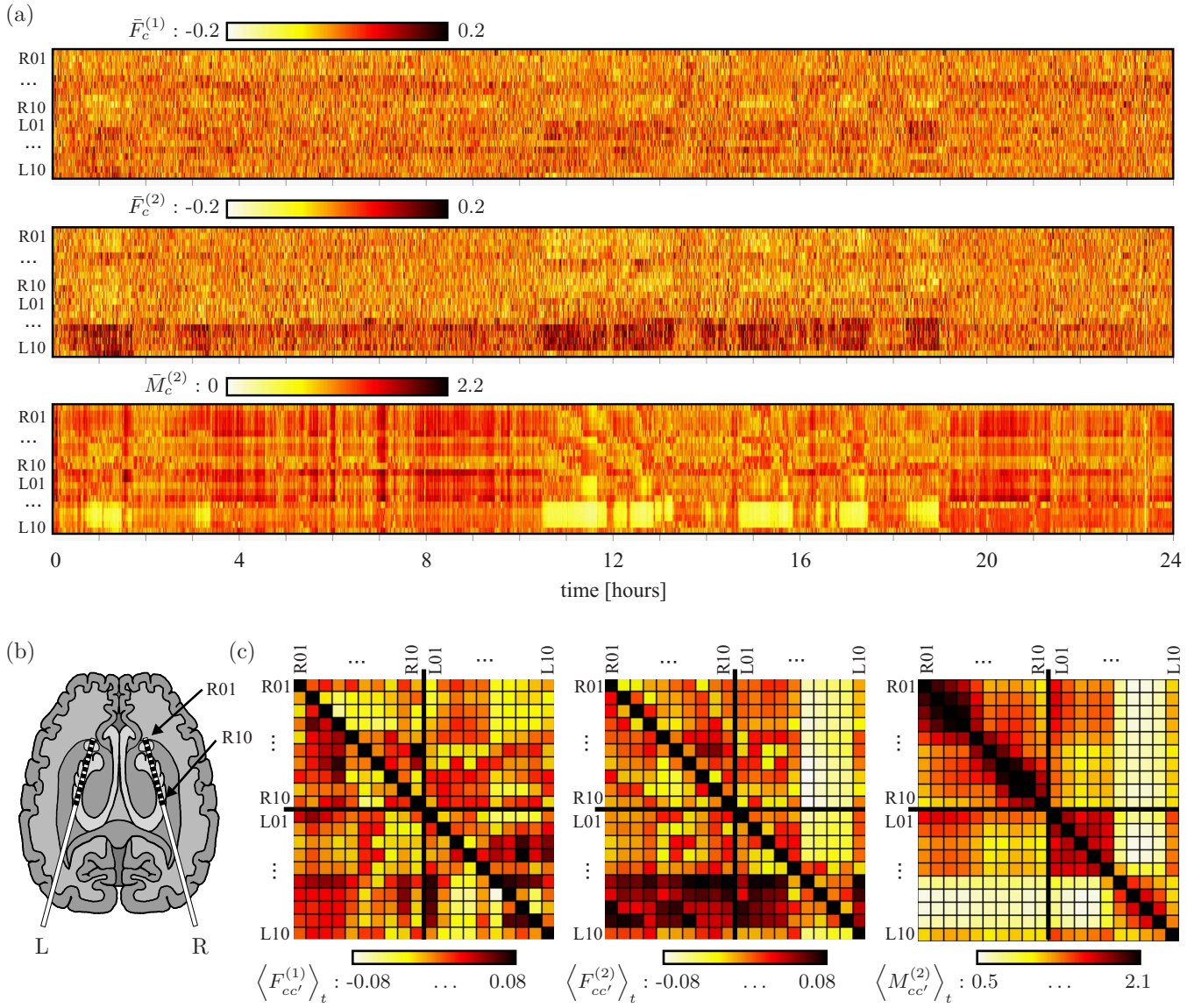

FIG. 5. (Color online) Exemplary results obtained from analyzing EEG data from a patient suffering from a left-sided focal epilepsy. (a) Section of the temporal evolution of the average interdependence between a given electrode contact and the remaining ones as quantified by $\bar{F}_c^{(1)}$ (top), $\bar{F}_c^{(2)}$ (middle), and $\bar{M}_c^{(2)}$ (bottom). The section started at 12:30 a.m. and covered 24 h. For $\bar{F}_c^{(1)}$ and $\bar{F}_c^{(2)}$ a positive value indicates that contact c has—on average—a weaker influence on the remaining contacts than vice versa. (b) Electrode implantation scheme for left (L) and right (R) intrahippocampal depth electrodes. Each electrode is equipped with ten cylindrical contacts (diameter 2.5 mm, intercontact distance 4 mm). (c) Temporal averages $\langle F_{cc'}^{(1)} \rangle_t$ (left), $\langle F_{cc'}^{(2)} \rangle_t$ (middle), and $\langle M_{cc'}^{(2)} \rangle_t$ (right) calculated from the entire EEG recording (duration 7 days). Data from the seizure-free interval entered the calculations only. A color-coded matrix entry with row and column indices c and c' represents the value of the respective measure calculated for an electrode contact combination (cc'), where $c,c' \in \{R01,\ldots,R10,L01,\ldots,L10\}$. A positive value of $\langle F_{cc'}^{(1)} \rangle_t$ or $\langle F_{cc'}^{(2)} \rangle_t$ indicates a stronger influence of contact c' on contact c than vice versa. Entries on the main diagonal are colored black.

Fokker-Planck coefficients in a one-dimensional framework. For these patients complete seizure control can be achieved by surgically removing the seizure generating brain structure. Since this structure could not be determined unequivocally with noninvasive diagnostic techniques, invasive EEG recordings via chronically implanted intrahippocampal depth electrodes [cf. Fig. 5(b)] were necessary before resective surgery. In four patients seizures originated exclusively from the left and in another four patients from the right temporal lobe. All patients achieved complete seizure control after surgery, so the epileptic focus can be assumed to be contained within the resected area. The EEG time series were sampled continuously over a longer period (5–12 days) with bandpass filter setting of 0.5–85 Hz (12 dB/octave) using a common average reference. The sampling interval Δt was 5 ms, and analog-digital conversion was performed at 16-bit resolution. All patients had signed informed consent that their clinical data might be used and published for research purposes, and the study was approved by the local medical ethics committee.

For each combination of the $N_c=20$ electrode contacts we performed a time resolved calculation of our interdependence measures using a moving-window technique with data windows of size $N=10\,000$ data points (corresponding to 50 s EEG) and windows overlapped by 50%. We restricted our analysis to EEG data from the seizure-free periods only; i.e., we excluded a possible preseizure period of 2 h duration, seizure activity, and a post-seizure period of 1 h duration. During EEG monitoring, patients had, on average, 6 seizures (range: 3–16 seizures). As in the case of our numerical studies presented in Sec. III we used $B=10$, $L=100$, and a fixed time shift of $\tau=1$ sampling interval.

In Fig. 5(a) we show, as an example, a section of the temporal evolution of the average interdependence between each contact c and the N_c-1 remaining ones quantified by

$$\bar{F}_c^{(1)}(w) = (N_c - 1)^{-1} \sum_{c' \neq c} F_{cc'}^{(1)}(w),$$

$$\bar{F}_c^{(2)}(w) = (N_c - 1)^{-1} \sum_{c' \neq c} F_{cc'}^{(2)}(w),$$

$$\bar{M}_c^{(2)}(w) = (N_c - 1)^{-1} \sum_{c' \neq c} M_{cc'}^{(2)}(w), \tag{13}$$

where, for example, $F_{cc'}^{(1)}(w)$ denotes the estimate of $F^{(1)}$ for window w and electrode contact combination (cc'). Despite fluctuations, we observed that with $F^{(2)}$ the brain region sampled with electrode contacts L06–L09 appears to be driven—on average—by the other brain regions (positive sign). With $F^{(1)}$ no such effect was discernible. Also the symmetric measure $M^{(2)}$ allowed one to detect this structure in the left hemisphere and may indicate a temporarily less pronounced mixing of noise processes in the EEG signals from this brain region. Although for this section of the data set the observed effects appeared to be most pronounced during night time (indicating a possible relationship to different states of vigilance), this was not a consistent finding for all patients.

In order to allow a compressed view of the presence and of the direction of interdependences between brain regions, we calculated, for each electrode contact combination (cc'), the quantities $\langle F_{cc'}^{(1)}\rangle_t$, $\langle F_{cc'}^{(2)}\rangle_t$, and $\langle M_{cc'}^{(2)}\rangle_t$, where $\langle\cdots\rangle_t$ denotes the average over all windows [cf. Fig. 5(c)]. Because of the antisymmetric definition of $F^{(1)}$ and $F^{(2)}$, the displays for the averaged quantities are antisymmetric, whereas the corresponding display for $M^{(2)}$ is symmetric. Given an EEG recording time of about 7 days for this patient, the averaged values are rather small. Nevertheless, with $F^{(2)}$ the highest average levels of interdependence during the seizure-free interval were again confined to the region sampled by electrode contacts L06–L09. Interestingly, this region corresponds to the epileptic focus as determined by established presurgical evaluation techniques [68]. Considering the sign of $F^{(2)}$, the epileptic focus seems to be driven even by brain regions from the opposite hemisphere. We could not observe a similar clear-cut interdependence structure with $F^{(1)}$. For this patient the lowest values of $M^{(2)}$ were confined to the same circumscribed brain region that corresponded to the epileptic focus.

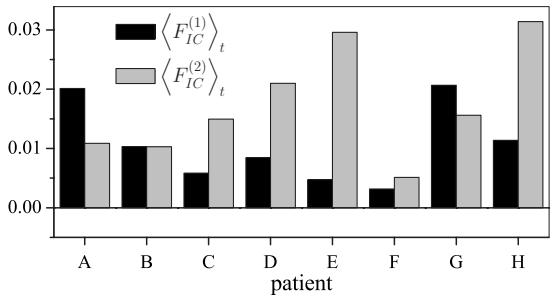

FIG. 6. Predominant direction of interdependences between the hemisphere containing the epileptic focus (*ipsilateral* hemisphere, *I*) and the opposite (*contralateral*, *C*) hemisphere as quantified by the temporal and spatial averages $\langle F_{IC}^{(1)}\rangle_t$ and $\langle F_{IC}^{(2)}\rangle_t$. For all patients, the positive values indicate a stronger influence of the contralateral on the ipsilateral hemisphere than vice versa.

We observed in six out of eight patients that with $F^{(2)}$ the epileptic focus—as determined by the presurgical workup—could be identified as a relatively narrow brain region that appeared to be influenced by all other sampled brain structures. With $F^{(1)}$ and $M^{(2)}$ such an identification was possible in one and three, respectively, patients only. We also considered the predominant direction of interdependences between the hemisphere containing the epileptic focus (*ipsilateral* hemisphere, *I*) and the opposite (*contralateral*, *C*) hemisphere by calculating the temporal and spatial averages

$$\langle F_{IC}^{(1)}\rangle_t = (N_c/2)^{-2} N_w^{-1} \sum_{c\in I, c'\in C, w} F_{cc'}^{(1)}(w),$$

$$\langle F_{IC}^{(2)}\rangle_t = (N_c/2)^{-2} N_w^{-1} \sum_{c\in I, c'\in C, w} F_{cc'}^{(2)}(w), \tag{14}$$

over all N_w analysis windows and all electrode contact combinations (cc'). Contacts c were from the ipsilateral and contacts c' from the contralateral brain hemisphere. Due to the crude spatial and temporal averaging, both $\langle F_{IC}^{(1)}\rangle_t$ and $\langle F_{IC}^{(2)}\rangle_t$ attained rather small values (cf. Fig. 6). Nevertheless, both quantities attained positive values in all patients, which indicates that the brain hemisphere containing the epileptic focus is being driven by the opposite hemisphere.

Summarizing this section, the findings presented here extend our previous observations using qualifiers that were based on estimated Fokker-Planck coefficients in a one-dimensional framework [42] by providing insights into the direction of interactions between the epileptic focus and other brain regions. When interpreting the estimator of $\mathbf{D}^{(2)}$ as the diffusion coefficient of a Fokker-Planck equation, our results indicate that a more detailed characterization of spatial (and temporal) aspects of the epileptic process can be achieved particularly when focusing on interactions in the stochastic part of the dynamics. Since the epileptic focus is usually assumed to drive other brain regions, our finding of an epileptic focus being almost constantly driven by other structures during the seizure-free interval might appear coun-

terintuitive or even contradictory. Although an unambiguous inference of directionality of interdependences from empirical data is far from being resolved [69], there are scenarios that might support our observations. One could, e.g., imagine that the driving reflects an inhibitory process that prevents the generation of a seizure within the epileptic network. Alternatively, the driving might also reflect an increased susceptibility of the seizure generating area within this network. These hypotheses are testable and should be investigated in future studies, which should include analyses of EEG data from a larger group of patients and a comparison with other approaches to assess directional interdependences.

V. CONCLUSION

We have proposed a data-driven method to characterize interdependences between dissipative dynamical systems under the influence of noise. For this purpose, we followed Refs. [29–31] to estimate drift and diffusion coefficients of a Fokker-Planck equation, and defined measures that are able to quantify the asymmetry in coupling as well as the presence of a mixing of the independent noise components of the process. We showed numerically that couplings in the deterministic part can be discriminated from couplings in the stochastic part of the dynamics if the coupling is not too strong and if effects of a potential usage of a finite time shift in the estimation of the coefficients are taken into account. We note that the definition of our measures does not depend on details of the procedure for estimating the coefficients. We used a finite time shift to facilitate a fully automated calculation of our interdependence measures. We could show that even for systems that do not meet the prerequisites needed for an analysis in terms of a two dimensional Fokker-Planck equation valuable information about the directionality of a coupling can be extracted using our approach.

Our results obtained from analyzing electroencephalographic recordings from epilepsy patients indicate that our approach can help to improve the evaluation of epilepsy patients candidate for respective therapies and to promote the current discussion as to whether human epilepsy can be regarded as a disorder of large neural networks [55,56]. We thus expect that our approach can contribute to further improve understanding of interdependences in complex dynamical systems such as the human brain even in cases where the assumptions underlying the Fokker-Planck approach (Markovianity, Gaussianity of the driving noise) might not be fulfilled in a strict sense.

ACKNOWLEDGMENTS

We are grateful to Holger Kantz, Joachim Peinke, and Stephan Bialonski for useful discussions and valuable comments. K.L. acknowledges support from the Deutsche Forschungsgemeinschaft (Grant No. SFB-TR3, sub-project A2 and LE660/4-1).

APPENDIX: INFLUENCE OF A FINITE TIME SHIFT τ ON THE ESTIMATION OF THE COEFFICIENTS

In order to investigate the influence of a finite time step on the estimation of the coefficients we followed Ref. [48] and considered the conditional moments in Eq. (6):

$$\mathbf{m}^{(n)}(\mathbf{x}',t,\tau) := \langle [\mathbf{X}(t+\tau)-\mathbf{X}(t)]^n \rangle|_{\mathbf{X}(t)=\mathbf{x}'} = \int d^n x (\mathbf{x}-\mathbf{x}')^n p(\mathbf{x},t+\tau|\mathbf{x}',t). \quad \text{(A1)}$$

Because $p(\mathbf{x},t+\tau|\mathbf{x}',t)$ is a solution of the Fokker-Planck equation $\partial_t p(\mathbf{x},t+\tau|\mathbf{x}',t)=\hat{L}p(\mathbf{x},t+\tau|\mathbf{x}',t)$, it can be expressed in terms of the Fokker-Planck operator $\hat{L}=-\Sigma_i \partial_{x_i} D^{(1)}+\Sigma_{ij}\partial_{x_i}\partial_{x_j}D^{(2)}$ (where $\partial_t=\partial/\partial t$ and $\partial_{x_i}=\partial/\partial x_i$) as

$$p(\mathbf{x},t+\tau|\mathbf{x}',t)=e^{\hat{L}\tau}\delta(\mathbf{x}-\mathbf{x}')=\sum_{k=0}^{\infty}\frac{(\hat{L}\tau)^k}{k!}\delta(\mathbf{x}-\mathbf{x}'), \quad \text{(A2)}$$

where $p(\mathbf{x},t|\mathbf{x}',t)=\delta(\mathbf{x}-\mathbf{x}')$ was used. Considering terms up to the order of τ^2 it follows for the ith component of the first conditional moment $(n=1)$,

$$m_i^{(1)}=\tau D_i^{(1)}+\frac{\tau^2}{2}\left(\sum_k D_k^{(1)}\partial_{x_k}D_i^{(1)}+\sum_{kl}D_{kl}^{(2)}\partial_{x_l}\partial_{x_k}D_i^{(1)}\right)+O(\tau^3), \quad \text{(A3)}$$

and for the entry with indices ij of the second conditional moment $(n=2)$,

$$m_{ij}^{(2)}=2\tau D_{ij}^{(2)}+\tau^2\left[D_i^{(1)}D_j^{(1)}+\sum_k\left(D_{jk}^{(2)}\partial_{x_k}D_i^{(1)}+D_{ik}^{(2)}\partial_{x_k}D_j^{(1)}\right)+\sum_k D_k^{(1)}\partial_{x_k}D_{ij}^{(2)}+\sum_{kl}D_{kl}^{(2)}\partial_{x_l}\partial_{x_k}D_{ij}^{(2)}\right]+O(\tau^3). \quad \text{(A4)}$$

If a coupling is present in the ith component of the drift vector, this component is a function of x_j—i.e., $D_i^{(1)}$

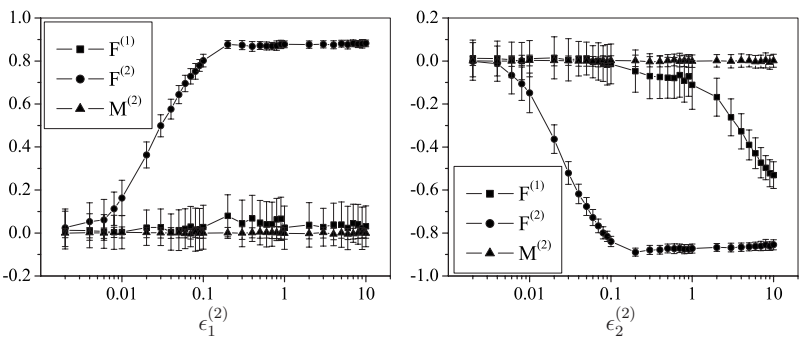

FIG. 7. Dependence of $F^{(1)}$, $F^{(2)}$, and $M^{(2)}$ on the coupling strength. Left: coupling of x_2 into $D_{11}^{(2)}$ and right: coupling of x_1 into $D_{22}^{(2)}$. Symbols and error bars denote means and standard deviations derived from 100 realizations of the respective processes. Time series consisted of $N=50\,000$ data points. Parameters in Eq. (11): $\alpha=\beta=0.1$, $g_{11}=g_{22}=0.1$, and $g_{12}=0.01$.

$=D_i^{(1)}(x_j)$. In this case the first term of order τ^2 in Eq. (A4) transfers this coupling to the entry ij of the estimated diffusion coefficient. Whether the other terms of order τ^2 in Eq. (A4) contribute to this effect depends on the functional characteristics of the first and second coefficients (i.e., it depends on whether the derivatives of $D_i^{(1)}$ and $D_j^{(1)}$ are still functions of x_j and on whether $\partial_{x_k} D_{ij}^{(2)} \neq 0$ in the third term of order τ^2). Thus, if the coupling strength and the time shift τ are large enough, the coupling can erroneously be detected by the measures $F^{(2)}$ and $M^{(2)}$ as is the case for the system shown in Fig. 2(a).

If a coupling is present in the ith diagonal element $D_{ii}^{(2)}$ of the diffusion coefficient, this coupling can only be transferred to the ith component of the estimated drift vector if the second derivative of $D_i^{(1)}$ does not vanish [cf. second term of order τ^2 in Eq. (A3)]. To demonstrate this effect we show in Fig. 7 results for the same system as in Fig. 2 but this time using a time shift that was larger by a factor of 10. For a coupling of the second process component x_2 into the first diagonal element of the diffusion coefficient [i.e., all coupling strengths were zero except $\epsilon_1^{(2)}$; cf. Fig. 7(a)] the coupling was not transferred to the estimated drift vector because $\partial_{x_1}^2(-\alpha x_1)=0$ and the second term of order τ^2 in Eq. (A3) did not contribute to the first component of the conditional moment. However, in the case a coupling of x_1 into the second diagonal element of the diffusion coefficient [i.e., all coupling strengths were zero except $\epsilon_2^{(2)}$; cf. Fig. 7(b)] the second derivative of $D_2^{(1)}$ is not zero—i.e., $\partial_{x_2}^2[x_2(\beta - x_2^2)] \neq 0$. Thus, the coupling was transferred to the estimated drift coefficient and was detected by the measure $F^{(1)}$.

[1] M. B. Priestley, *Nonlinear and Non-Stationary Time Series Analysis* (Academic Press, London, 1988).
[2] J. S. Bendat and A. G. Piersol, *Random Data Analysis and Measurement Procedure* (Wiley, New York, 2000).
[3] A. S. Pikovsky, M. G. Rosenblum, and J. Kurths, *Synchronization—A Universal Concept in Nonlinear Sciences* (Cambridge University Press, Cambridge, England, 2001).
[4] S. Boccaletti, J. Kurths, G. Osipov, D. L. Valladares, and C. S. Zhou, Phys. Rep. **366**, 1 (2002).
[5] E. Pereda, R. Quian Quiroga, and J. Bhattacharya, Prog. Neurobiol. **77**, 1 (2005).
[6] K. Hlaváčková-Schindler, M. Paluš, M. Vejmelka, and J. Bhattacharya, Phys. Rep. **441**, 1 (2007).
[7] M. G. Rosenblum and A. S. Pikovsky, Phys. Rev. E **64**, 045202(R) (2001).
[8] D. A. Smirnov and B. P. Bezruchko, Phys. Rev. E **68**, 046209 (2003).
[9] L. Cimponeriu, M. Rosenblum, and A. Pikovsky, Phys. Rev. E **70**, 046213 (2004).
[10] D. A. Smirnov and R. G. Andrzejak, Phys. Rev. E **71**, 036207 (2005).
[11] B. Schelter, M. Winterhalder, R. Dahlhaus, J. Kurths, and J. Timmer, Phys. Rev. Lett. **96**, 208103 (2006).
[12] B. Kralemann, L. Cimponeriu, M. Rosenblum, A. Pikovsky, and R. Mrowka, Phys. Rev. E **76**, 055201(R) (2007).
[13] H. Osterhage, F. Mormann, T. Wagner, and K. Lehnertz, Int. J. Neural Syst. **17**, 139 (2007).
[14] D. A. Smirnov, M. B. Bodrov, J. L. Perez Velazquez, R. A. Wennberg, and B. P. Bezruchko, Chaos **15**, 024102 (2005).
[15] D. Smirnov, B. Schelter, M. Winterhalder, and J. Timmer, Chaos **17**, 013111 (2007).
[16] S. J. Schiff, P. So, T. Chang, R. E. Burke, and T. Sauer, Phys. Rev. E **54**, 6708 (1996).
[17] J. Arnhold, P. Grassberger, K. Lehnertz, and C. E. Elger, Physica D **134**, 419 (1999).
[18] R. Quian Quiroga, J. Arnhold, and P. Grassberger, Phys. Rev. E **61**, 5142 (2000).
[19] M. C. Romano, M. Thiel, J. Kurths, and C. Grebogi, Phys. Rev. E **76**, 036211 (2007).
[20] T. Schreiber, Phys. Rev. Lett. **85**, 461 (2000).
[21] M. Paluš, V. Komárek, Z. Hrnčíř, and K. Štěrbová, Phys. Rev. E **63**, 046211 (2001).
[22] M. Żochowski and R. Dzakpasu, J. Phys. A **37**, 3823 (2004).
[23] L. Gammaitoni, P. Hänggi, P. Jung, and F. Marchesoni, Rev. Mod. Phys. **70**, 223 (1998).
[24] F. Sagues, J. M. Sancho, and J. Garcia-Ojalvo, Rev. Mod. Phys. **79**, 829 (2007).
[25] H. Nakao, K. Arai, and Y. Kawamura, Phys. Rev. Lett. **98**, 184101 (2007).
[26] H. Risken, *The Fokker-Planck Equation*, 2nd ed. (Springer, Berlin, 1989).
[27] N. G. van Kampen, *Stochastic Processes in Physics and Chemistry* (North-Holland, Amsterdam, 1981).
[28] P. Hänggi and H. Thomas, Phys. Rep. **88**, 207 (1982).
[29] R. Friedrich and J. Peinke, Phys. Rev. Lett. **78**, 863 (1997).
[30] S. Siegert, R. Friedrich, and J. Peinke, Phys. Lett. A **243**, 275 (1998).
[31] R. Friedrich, S. Siegert, J. Peinke, S. Lück, M. Siefert, M. Lindemann, J. Raethjen, G. Deuschl, and G. Pfister, Phys. Lett. A **271**, 217 (2000).
[32] S. Lück, J. Peinke, and R. Friedrich, Phys. Rev. Lett. **83**, 5495 (1999).
[33] J. Gradisek, S. Siegert, R. Friedrich, and I. Grabec, Phys. Rev. E **62**, 3146 (2000).
[34] C. Renner, J. Peinke, and R. Friedrich, J. Fluid Mech. **433**, 383 (2001).
[35] H. U. Bödeker, M. C. Röttger, A. W. Liehr, T. D. Frank, R. Friedrich, and H.-G. Purwins, Phys. Rev. E **67**, 056220 (2003).
[36] M. Waechter, F. Riess, H. Kantz, and J. Peinke, Europhys. Lett. **64**, 579 (2003).
[37] G. R. Jafari, S. M. Fazeli, F. Ghasemi, S. M. Vaez Allaei, M. R. Tabar, A. Iraji Zad, and G. Kavei, Phys. Rev. Lett. **91**, 226101 (2003).
[38] T. D. Frank, P. J. Beek, and R. Friedrich, Phys. Lett. A **328**, 219 (2004).
[39] T. Kuusela, T. Shepherd, and J. Hietarinta, Phys. Rev. E **67**, 061904 (2003).
[40] T. Kuusela, Phys. Rev. E **69**, 031916 (2004).
[41] A. M. van Mourik, A. Daffertshofer, and P. J. Beek, Biol.

Cybern. **94**, 233 (2006).
[42] J. Prusseit and K. Lehnertz, Phys. Rev. Lett. **98**, 138103 (2007).
[43] M. Siefert, A. Kittel, R. Friedrich, and J. Peinke, Europhys. Lett. **61**, 466 (2003).
[44] F. Böttcher, J. Peinke, D. Kleinhans, R. Friedrich, P. G. Lind, and M. Haase, Phys. Rev. Lett. **97**, 090603 (2006).
[45] M. Siefert and J. Peinke, J. Turbul. **7**, 1 (2006).
[46] P. E. Kloeden and E. Platen, *Numerical Solution of Stochastic Differential Equations* (Springer, Berlin, 1999).
[47] In preliminary investigations we could not observe a strong influence of the specific choice of B and L as long as $B>4$ and $L>20$ and not too large. For different model systems and for time series that consisted of $5000 \leq N \leq 100\,000$ data points, $B=10$ and $L=100$ turned out to be a good choice.
[48] R. Friedrich, C. Renner, M. Siefert, and J. Peinke, Phys. Rev. Lett. **89**, 149401 (2002).
[49] P. Sura and J. Barsugli, Phys. Lett. A **305**, 304 (2002).
[50] M. Ragwitz and H. Kantz, Phys. Rev. Lett. **87**, 254501 (2001).
[51] O. E. Rössler, Phys. Lett. **57A**, 397 (1976).
[52] M. G. Rosenblum, A. S. Pikovsky, and J. Kurths, Phys. Rev. Lett. **76**, 1804 (1996).
[53] Z. Zheng and G. Hu, Phys. Rev. E **62**, 7882 (2000).
[54] F. Rosenow and H. Lüders, Brain **124**, 1683 (2001).
[55] S. S. Spencer, Epilepsia **43**, 219 (2002).
[56] M. Guye, J. Régis, M. Tamura, F. Wendling, A. Mc Gonigal, P. Chauvel, and F. Bartolomei, Brain **129**, 1917 (2006).
[57] F. Bartolomei, F. Wendling, J.-J. Bellanger, J. Régis, and P. Chauvel, Clin. Neurophysiol. **112**, 1746 (2001).
[58] F. Bartolomei, F. Wendling, J. Régis, M. Gavaret, M. Guye, and P. Chauvel, Epilepsy Res. **61**, 89 (2004).
[59] M. A. B. Brazier, Exp. Neurol. **36**, 263 (1972).
[60] W. Gersch and G. V. Goddard, Science **169**, 701 (1970).
[61] H. P. Zaveri, W. J. Williams, J. C. Sackellares, A. Beydoun, R. B. Duckrow, and S. S. Spencer, Clin. Neurophysiol. **110**, 1717 (1999).
[62] W. Gersch, Math. Biosci. **14**, 177 (1972).
[63] M. Le Van Quyen, C. Adam, M. Baulac, J. Martinerie, and F. Varela, Brain Res. **792**, 24 (1998).
[64] D. Krug, H. Osterhage, C. E. Elger, and K. Lehnertz, Phys. Rev. E **76**, 041916 (2007).
[65] M. Le Van Quyen, J. Martinerie, C. Adam, and F. J. Varela, Physica D **127**, 250 (1999).
[66] J. P. Pijn and F. Lopes da Silva, in *Basic Mechanisms of the EEG*, edited by S. Zschocke and E.-J. Speckmann (Birkhäuser, Boston, 1993), p. 41.
[67] H. Osterhage, F. Mormann, T. Wagner, and K. Lehnertz, Phys. Rev. E **77**, 011914 (2008).
[68] J. Engel, Jr. and T. A. Pedley, *Epilepsy: A Comprehensive Textbook*, 2nd ed. (Lippincott, Williams & Wilkins, Philadelphia, 2007).
[69] M. Paluš and M. Vejmelka, Phys. Rev. E **75**, 056211 (2007).